Mesoporous TiO_2 from poly(N,N-dimethylacrylamide)-b-polystyrene block copolymers for long-term acetaldehyde photodegradation

Mesoporous TiO_2 from poly(N,N-dimethylacrylamide)-b-polystyrene block copolymers for long-term acetaldehyde photo degradation

Jonas Billet[1,2], Stef Vandewalle[2], Mieke Meire[1], Natan Blommaerts[3], Petra Lommens[1], Sammy W. Verbruggen[3], Klaartje De Buysser[1], Filip Du Prez[2], Isabel Van Driessche[1,*]

[1]*Department of Chemistry, Sol–gel Centre for Research on Inorganic Powders and Thin films Synthesis (SCRiPTS), Ghent University, Krijgslaan 281 (S3), 9000 Ghent, Belgium*

[2]*Polymer Chemistry Research group, Centre of Macromolecular Chemistry (CMaC), Department of Organic and Macromolecular Chemistry, Faculty of Sciences, Ghent University, Krijgslaan, 281 (S4-bis), B-9000 Ghent, Belgium*

[3]*Department of Bioscience Engineering, University of Antwerp, Groenenborgerlaan 171, 2020 Antwerp, Belgium*

Abstract

Although already some mesoporous (2 – 50 nm) sol-gel TiO_2 synthesis strategies exist, no pore size control beyond the 12 nm range is possible without using specialized organic structure directing agents synthetized via controlled anionic/radical polymerizations. Here we present the use of reversible addition-fragmentation chain transfer (RAFT) polymerization as a straightforward and industrial applicable alternative to the existing controlled polymerization methods for structure directing agent synthesis. Poly(N,N-dimethylacrylamide)-*block*-polystyrene (PDMA-*b*-PS) block copolymer, synthesized via RAFT, was chosen as structure directing agent for the formation of the mesoporous TiO_2. Crack-free thin layers TiO_2 with tunable pores from 8 to 45 nm, could be acquired. For the first time, in a detailed and systematic approach, the influence of the block size and dispersity of the block copolymer is experimentally screened for their influence on the final meso-TiO_2 layers. As expected, the mesoporous TiO_2 pore sizes showed a clear correlation to the polystyrene block size and the dispersity of the PDMA-b-PS block copolymer. Surprisingly the dispersity of the polymer was shown not to be affecting the standard deviation of the pores. As a consequence RAFT could be seen as a viable alternative to the aforementioned controlled polymerization reactions for the

synthesis of structure directing agents enabling the formation of mesoporous pore-size controlled TiO_2. To examine the photocatalytic activity of the mesoporous TiO_2 thin layers the degradation of acetaldehyde, a known indoor pollutant, was studied. Even after three years of aging, the TiO_2 thin layer retained most of its activity.

Keywords:

RAFT, Block copolymer, PDMA-*b*-PS, Mesoporous, TiO2, Sol-gel

Introduction

Mesoporous materials, mostly silica, are widely used for their unique catalytic and adsorption properties [1]. In case of silica, the very high surface areas, its uniform pore structure and the wide range of surface functionalities offer huge potential. Over the last two decades, the same approach of mesostructuring has been extended to other oxides such as ZrO_2, Al_2O_3, Nb_2O_5, TiO_2,...[2-4]. Particularly titania (TiO_2) exhibits excellent properties as photocatalyst [5-8], and is suited for applications such as (dye-sensitized) solar cells [9-11], catalyst (support) [12], gas sensing [13], Li-ion insertion [14,15]. Most of these applications require a high specific surface, a high crystallinity, controllable pore-dimensions and the formation of crack-free layers when implemented as thin films. Unfavorable pore dimensions (pore diameter, volume and neck diameter) will have a detrimental effect on the applicability of porous TiO_2, and pore dimensions should be tuned for every application [16-18].

Following the successful silica structuring methods, porous TiO_2 is mostly synthesized using soft-templated methods in which an organic structure directing agent (SDA) is mixed with an Ti-precursor under acidic conditions (Scheme 1). The hydrophilic section of the amphiphilic SDA interacts with the inorganic entities through H-bonding/electrostatic interaction whilst the pore-forming hydrophobic section separates the hydrophilic components with nanoscale periodicity [6]. During the evaporation of the solvent in the coating procedure, the inorganic-organic pore system self-assembles by evaporation induced self-assembly (EISA). Finally the mesoporous titania is obtained after calcination at high temperatures. These soft-templating methods give an unprecedented degree of control over the size, shape, and spatial arrangement of the pores compared to hard templating or without template methods [19]. The first, and still most, used SDA's are cetyltrimethylammonium bromide, Brij 56-58 and Pluronic® molecules/polymers. These commercial SDA's give pores in the limited size range of 1-12 nm, depending on the synthetic conditions [20-22,1]. The activity of the mesoporous TiO_2, in applications where device performance directly depends on the pore size of the porous structure [17],[18], will improve beyond this 12 nm threshold.

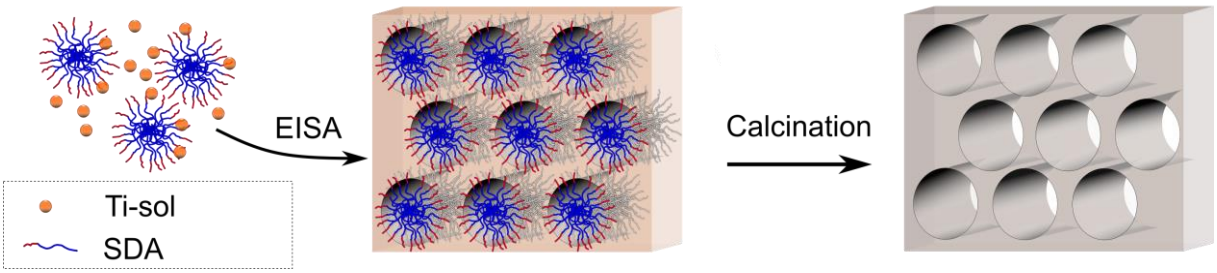

Scheme 1: Synthesis of mesoporous TiO_2 through the evaporation induced self-assembly (EISA) of a Ti-precursor with the structure directing agent (SDA). The porous TiO_2 structure is obtained after calcination to remove the organic SDA template.

Synthesizing mesoporous (2-50 nm pores) TiO_2 beyond the 12 nm threshold is challenging with commercial SDA's, but with the introduction of poly(ethylene-co-butylene)-*b*-polyethylene oxide block copolymers (BCPs) by Sanchez et.al. [4], pore sizes in a larger range (5 -50 nm) could be reached by varying the block's sizes. Since then, an array of amphiphilic di and tri-block copolymers have been synthesized by other pioneers like Wiesner and Stefik: poly(ethylene oxide)-*b*-poly(hexylacrylate) [23], poly(isoprene)-*b*-poly(ethylene oxide) [24], polystyrene-*b*-poly(ethylene oxide) [25,5,14], poly(isoprene)-*b*-polystyrene-*b*-poly(ethylene oxide) [24], poly(methyl methacrylate)-*b*-poly(ethylene oxide) [26], polystyrene-*b*-poly(acrylic acid) [27,28] and polystyrene-*b*-poly(4-vinylpyridine) [13]. In most of these amphiphilic block copolymers poly(ethylene oxide) is chosen as the inorganic tethering domain due to its relative hydrophilicity, its easiness to form (block co-)polymers and its ability to form crown ether like interactions through weak coordination bonds with Ti-ions [23,2].

By synthesizing a block copolymer with a narrow dispersity (Đ), the eventual meso-TiO_2 pore size and the assembly of the Ti-sol and the BCP can be controlled [29-31]. To achieve this control, the templates are mostly synthesized by living anionic polymerization, which gives polymers with very low dispersity values (1.01 -1.05). However, anionic polymerizations require intensive purification of all reagents and tedious experimental conditions [32,33]. Therefore, more recently, work has been performed to facilitate the synthesis of BCPs via reversible deactivation radical polymerization (RDRP) methods, which are far more tolerant to given reaction conditions and are able to control the polymerization of more monomers that can be beneficial to prepare various block copolymers [32]. The most popular RDRP technique for the synthesis of the aforementioned structure directing agents is atom transfer radical polymerization (ATRP) that makes use of a copper complex to control the radical process [34,6]. Another RDRP technique that is frequently used for the synthesis of block copolymers is reversible addition-fragmentation chain transfer (RAFT) polymerization [35,36]. Compared to ATRP, RAFT has the advantage that its kinetics and reaction conditions are analogous to

free radical polymerization. Indeed, the only difference in the reaction set-up is the addition of a chain transfer reagent that is able to control the radical polymerization [37]. As such, the technique could easily be implemented in presently used industrial polymerization reactors, under routine temperatures, times and pressures. Added to easy reaction set-up, RAFT is compatible with a broad range of functionalities [33] and all the RAFT foundation patents have expired at the end of 2018 [38]. The downside of using RAFT is its inability to avoid small quantities of polymer defects, such as dead (co)polymers, which can have an effect on the dispersity of the block copolymers. In other applications of block copolymers, like lithography, the dispersity was shown to have an extensive unfavorable influence on its self-assembled structure [39]. However the assessment of the influence of a slightly higher dispersity of RAFT-synthesized block copolymer SDA on the metal oxide mesoporous structure and pore variance has not been made yet. If the marginally increased dispersity would prove to be only of negligible influence, the economic advantages of synthesizing the SDA's via RAFT can be implemented.

Several factors have to be taken into account when designing a new structure-directing block copolymer for the synthesis of mesoporous TiO_2 [40]. (1) A narrow dispersity of the SDA induces pore control and consistent self-assembled structures [30]. (2) A high polymer-polymer Flory-Huggins interaction parameter χ_{AB} [41], which is indicative of a significant hydrophobic-hydrophilic contra of the polar- apolar A-B blocks of the copolymer, leads to a profound phase separation of the blocks and thus will more easily induce pore formation. (3) By kinetically entrapping the micelles, their rearrangement during film processing is avoided, which is achieved by a distinctive Flory-Huggins parameter χ_{1B} between the solvent and the hydrophobic polymer, *e.g.* block segment B can be (almost) insoluble in the main solvent (4) The precipitation of the polymer or the Ti-precursor during evaporation, can be avoided by the correct choice of solvent system. Solubility of the block copolymer in the H-bonding solvents THF/DMF is of particular interest, as these solvents can easily be incorporated into meso-TiO_2 precursor solutions [24]. Lastly, (5) the Ti-sol should be able to interact with the hydrophillic part of the block copolymer.

Here, we demonstrate the use of poly(N,N-dimethylacrylamide)-*b*-polystyrene (PDMA-*b*-PS) block copolymer, synthesized via RAFT, as SDA in the synthesis of coated mesoporous TiO_2. PDMA was chosen as a Ti-sol tethering domain, as the DMF-like H-bonding with Ti is mimicked [42]. which results in a profound interaction between the Ti-precursor and the PDMA segment [43]. By opting for polystyrene as solvophobic block and EtOH as main solvent, χ_{1B}

(between the solvent and the hydrophobic polymer) is maximized, which kinetically entraps the formed micelles [13,44]. The effect of the dispersity and the size of the block copolymer segments on the variance and size of the mesopores is statistically investigated. As a proof of concept, the photocatalytic activity of the thin layers was assessed by following the degradation of gaseous acetaldehyde.

Materials and methods

Poly(N,N-dimethylacrylamide)-*b*-polystyrene synthesis

Poly(N,N-dimethylacrylamide)-*b*-polystyrene was synthesized *via* RAFT copolymerization in two steps. First the PDMA block was prepared using 2-([(butylsulfanyl)-carbonothioyl]sulfanyl)propanoic acid as chain transfer agent, which was synthesized as previously reported.[45] Then, the formed and fully purified PDMA-based macro-RAFT agent was used in the RAFT polymerization of styrene, as depicted in Scheme 2. A detailed procedure is given below.

For the synthesis of a PDMA-based macro RAFT agent with a molecular weight of 5000 g/mol, DMA (70 eq., 5 mL), initiator azobisisobutyronitrile (AIBN) (0.11 eq., 12.5 mg), 2-([(butylsulfanyl)-carbonothioyl]sulfanyl)propanoic acid (1eq., 0.165g) and dimethylformamide (DMF, 5 mL) were mixed in a Schlenk tube. The tube was deoxygenated by performing three freeze-pump-thaw cycles and was immersed in an oil bath at 65 °C for 4 h. The reaction was quenched by submersing the Schlenk tube in liquid nitrogen. The polymer was isolated by removing the DMF under reduced pressure, followed by dissolving the polymer mixture in tetrahydrofuran (THF, 2 mL) and precipitating in diethyl ether (20 mL). The resulting polymer was filtered and finally dried under reduced pressure at 40 °C (12 h) and characterized by size-exclusion chromatography (SEC), and ^{1}H nuclear magnetic resonance (NMR) analysis.

For a typical copolymerization of PS, the PDMA-based macro-RAFT agent (1 eq, 1 g, 0.2 mmol), AIBN initiator (0.11eq, 3.54 mg), styrene (300 eq, 6.7 mL), and DMF (10 mL) were added to a Schlenk tube. The solution was deoxygenated with three freeze-pump-thaw cycles. The flask was immersed in an oil bath at 90 °C for 24 hours. The polymerization reaction was stopped by submersing the Schlenk tube in liquid nitrogen. After removing the DMF fraction under reduced pressure, the block copolymer was isolated by dissolving in THF (5 mL) and precipitating the polymer into heptane (50 mL). The resulting polymer was filtered and dried under reduced pressure at 40 °C over 12 h and characterized by SEC and ^{1}H NMR analysis.

EISA synthesis of mesoporous TiO_2 with PDMA-*b*-PS

The recipe described by Beyers *et al.*[21] for the synthesis of mesoporous TiO_2 using Pluronic templates was altered for PDMA-*b*-PS. In a typical synthesis, 0.1g of PDMA-*b*-PS polymer is dissolved in 1 mL THF. Kinetically trapped micelles are formed by the dropwise addition of 2 mL EtOH ($0.5 mL min^{-1}$), forming a slightly turbid solution. After 1 h of rigorous stirring, 0.75 mL of HCl solution and 0.313 mL of $Ti(OiPr)_4$ is added, forming an orange colored marginally

unclear solution. The resulting mixture is again stirred for 4 h and spin coated on square 4 cm^2 Si substrates at 35% humidity and 25 °C. The thin films were heat treated for 30 min at 65 °C to induce full solvent evaporation. The calcination of the film proceeds for 2 h at 450 °C with a heating rate of 2 $°Cmin^{-1}$.

To obtain a mesoporous powder, the same precursor solution is aged for 1 h, transferred to a Petri dish and dried in an oven at 65 °C for 3 days. The obtained yellow solid powder is isolated, washed 3 times with distilled water, dried overnight at ambient conditions, and finally calcined for 2h at 450 °C with a heating rate of 2 $°Cmin^{-1}$.

Statistical analysis

All analyses were conducted in R version 3.5.1. Normality of distribution were verified using QQ-plots, and P-values below 0.05 were established as statistically significant. All regression results are given in the supporting information.

Photocatalytic activity test

Acetaldehyde (AcAl) was used as a model pollutant for indoor air contamination. A polluted gas flow was generated by pre-mixing 1% AcAl in N_2 (Praxair) with synthetic air (Praxair), resulting in an AcAl concentration of (30 ± 3) ppmv. The thin films samples (2 cm at 2 cm) were placed in the center of a single pass, 150 mm x 20 mm x 2.75 mm slit-shaped flatbed photoreactor as described in earlier work [46-48]. A Philips Cleo UVA lamp (λ_{max} = 365 nm, 25W, incident intensity of 3mW cm^{-2} at a sample distance of 2 cm was used as light source. In line with earlier work, the measurements were carried out according to the following validated procedure: (1) The dark reactor is flushed with clean air. (2) The reactor is illuminated and flushed with clean air. During this step the adsorbed rest fractions from the synthesis or coating protocols are photocatalytically removed from the substrate. (3) The pollutant reference level is determined by measuring the polluted air directly in the detector, not through the reactor but by the bypass. (4) Measuring the adsorption of the substrates by passing the polluted air through the dark reactor. (5) The reactor is illuminated and the photocatalytic activity is monitored. The concentration levels of AcAl and CO_2 are monitored in-line and in *quasi* real-time by Fourier transform infrared (FTIR) spectroscopy. The FTIR absorbance is converted into an actual concentration using pre-established calibration curves, constructed using an organic vapor sensor and CO_2 sensor. For each sample an automated test protocol is run, using the previously described cycles, three consecutive times, with 15 minutes polluted flow through the reactor in the dark and 20 minutes under UV illumination.

Characterization

Powder X-ray diffraction (PXRD) patterns of the powders were collected on a Thermo Scientific ARL XTra diffractometer, operated at 40 kV, 40 mA using Cu Kα radiation. NMR measurements were recorded on a Bruker Avance lll spectrometer operating at a ^{1}H frequency of 500.13 MHz and equipped with a BBI-Z probe. The sample temperature was set at 298.2 K. SEC-DMA was performed on a Agilent 1260-series HPLC system equipped with a 1260 online degasser, a 1260 ISO-pump, a 1260 automatic liquid sampler (ALS), a thermostatted column compartment (TCC) at 50°C equipped with a PSS Gram30 column in series with a PSS Gram1000 column, a 1260 diode array detector (DAD) and a 1260 refractive index detector (RID). The used eluent was dimethylacetamide containing 50 mM of LiCl at a flow rate of 1 mL/min. The spectra were analyzed using the Agilent Chemstation software with the SEC add on. Molar mass and PDI values were calculated against Varian PS standards. SEC-THF was performed using a Varian PLGPC50plus instrument, using a refractive index detector, equipped with two Plgel 5 µm MIXED-D columns 40 °C. Polystyrene standards were used for calibration and THF as eluent at a flow rate of 1 $mLmin^{-1}$. Samples were injected using a PL AS RT autosampler. Thermogravimetric analyses were performed with a Mettler-Toledo TGA/SDTA 851e instrument. The measurements were performed under air with a heating rate of 10 $Kmin^{-1}$ from 25 °C to 800 °C on samples with sizes of 5-10 mg. Mettler-Toledo STARe software was used to analyze the thermograms. Samples were measured with GC to determine the monomer conversion from the ratio of the integrals from the monomer and the internal standard, DMF. GC was performed on an Agilent 7890A system equipped with a VWR Carrier-160 hydrogen generator and an Agilent HP-5 column of 30 m length and 0.320 mm diameter. An FID detector was used and the inlet was set to 240 °C with a split injection of ratio 25:1. Hydrogen was used as carrier gas at a flow rate of 2 $mLmin^{-1}$. The oven temperature was increased with 20°C/min from 50°C to 120°C, followed by a ramp of 50°C/min to 150°C.

Nitrogen sorption experiments were carried out on a TriStar 3000 (Micromeritics) at -196 °C. The specific surface areas were calculated using the Brunauer-Emmett- Teller (BET) method. FTIR (DRIFTS) spectra were recorded on a Nicolet6700 FTIR spectrometer (Thermo-Scientific) equipped with MCTdetector (analyses performed at 100 °C under vacuum). The scanning electron microscope (SEM) images were recorded on a JEOL JSM7600F, operated at 10 kV and a current of 6 A. The morphology and composition information of the layer were observed via high-angle annular dark-field scanning transmission electron microscopy (HAADF-STEM) technique using a *Cs*-corrected JEOL JEM 2200-FS instrument operated at

200 kV and energy-dispersive x-ray spectroscopy. Lamella for HAADF-STEM were prepared by cutting a cross-sectional lamella via the Focused Ion Beam (FIB) technique in a FEI Nova 600 Nanolab Dual Beam FIB scanning electron microscopy [49]. The lamella were extracted using the in situ lift out procedure with an Omniprobe extraction needle.

Results and Discussion

Design and synthesis of PDMA-b-PS

The PDMA-b-PS block copolymers were synthesized by RAFT polymerization as depicted in Scheme 2. First, the PDMA-based macro-RAFT agent was prepared by performing the RAFT polymerization of DMA using 2-([(butylsulfanyl)-carbonothioyl]sulfanyl)propanoic acid as chain transfer agent, a frequently applied trithiocarbonate that performs well for the controlled polymerization of acrylates, acrylamide and styrene[37]. In a second step, the PDMA-based macro-RAFT agent is purified and used for the copolymerization with styrene to obtain well-defined PDMA-*b*-PS block copolymers.

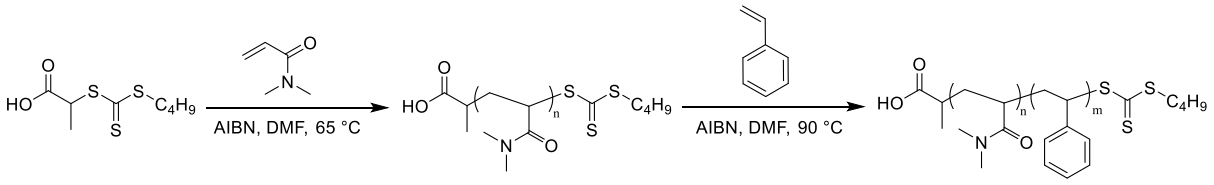

Scheme 2: RAFT polymerization of PDMA-*b*-PS; by the formation of a PDMA-macro RAFT transfer agent with 2-([(butylsulfanyl)-carbonothioyl]sulfanyl)propanoic acid as chain transfer agent and its subsequent polymerization with styrene.

A small library of PDMA-*b*-PS block copolymers were synthesized using this strategy. The respective molar masses and dispersity, as obtained from ^{1}H NMR and SEC analysis are listed in Table 1. The 1H NMR spectra, FTIR and SEC traces of all block copolymers are attached in the supporting information (Fig S1-9). The theoretical mass of the PDMA block copolymer segment was calculated based on the N,N-dimethylacrylamide conversion as obtained from GC analysis. The polymerization reactions leading to $PDMA_{5.7k}$ and $PDMA_{8k}$ were stopped at 75% and 60% conversion, respectively in order to minimize the side reactions and keep a good control over the polymerization process and thus obtain a narrow dispersity.

The theoretical molecular weight of the polystyrene block is calculated from the integration of resonance assigned to PS (Fig 1 A, Fig S2-9) from ^{1}H NMR analysis. The ratio of the PS block copolymer segment is calculated from the integration of the resonances, corresponding to the 5 hydrogen atoms on the benzene ring of styrene (Fig 1 A: *e*, *f* and *g*), and the integration of the resonance corresponding to the 6 hydrogen atoms of the 2 methyl groups of PDMA (Fig 1 A: *j*). From the theoretical mass of the PDMA block copolymer, obtained from GC analysis, and the PDMA/PS ratio, the theoretical molecular weight of the polystyrene block is obtained and listed in Table 1.

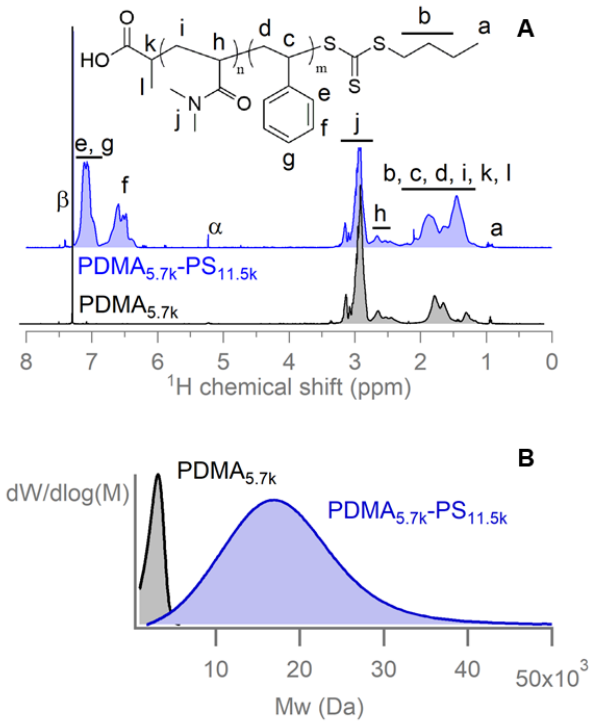

Figure 1: A : ^{1}H NMR spectrum of PDMA5.7k and PDMA$_{5.7k}$-*b*-PS$_{11.5k}$ in $CDCl_3$. The beta resonance refers to chloroform, while the alpha resonance corresponds to a CH_2Cl_2 impurity. **B**: THF-SEC analysis of PDMA$_{5.7k}$ and PDMA$_{5.7k}$-PS$_{11.5k}$. Due to its ability to form H-bonds in the THF solvent, the PDMA polymer chain appears to be smaller compared to the PS standards used in SEC analysis.

Finally, the dispersity of the PDMA-b-PS is obtained from THF-SEC analysis (Fig 1 B, Fig S2-9). Due to the ability of the PDMA block to form intra-chain H-bond, the molecular weights obtained from THF-SEC and ^{1}H NMR differs and the molecular weight and dispersity both appeared to be smaller (Fig 1 B). The dispersity of the PDMA block was obtained from DMA-SEC (Fig S1 D/S6 D), where these H-bonds were interrupted by the addition of LiCl salt in the solvent that was used for SEC analysis.

Table 1 : PDMA-b-PS block copolymers, with their respective molar masses and dispersity indices. The final composition of the block copolymer segments was determined from the ratio of the intensities of distinctive PDMA and PS ^{1}H NMR signals, as depicted in Figure 1. [a]Theoretical molecular weight as calculated from N,N-dimethylacrylamide conversion by GC. [b]Determined by SEC analysis using dimethylacetamide with 50 mM LiCl as solvent. [c]Determined by ^{1}H NMR analysis. [d]Determined by SEC analysis using THF as solvent .

Block copolymer	PDMA$_{5.7k}$ PS$_{7k}$	PDMA$_{5.7k}$ PS$_{11.5k}$	PDMA$_{5.7k}$ PS$_{14k}$	PDMA$_{5.7k}$ PS$_{30k}$	PDMA$_{8k}$ PS$_{8k}$	PDMA$_{8k}$ PS$_{17k}$	PDMA$_{8k}$ PS$_{21k}$
PDMA-macro RAFT							
[DMA]/[CTA]/[I]	75/1/0.11	75/1/0.11	75/1/0.11	75/1/0.11	140/1/0.11	140/1/0.11	140/1/0.11
$M_{n,theor}$[a]	5700	5700	5700	5700	8000	8000	8000
$M_{n,SEC}$[b]	4900	4900	4900	4900	5500	5500	5500
Đ[b]	1.2	1.2	1.2	1.2	1.30	1.30	1.30
PDMA-*b*-PS							
[Sty]/[Macro RAFT]/[I]	150/1/0.11	225/1/0.11	300/1/0.11	550/1/0,11	400/1/0.11	800/1/0.11	10^3/1/0.11

$M_{n,theor}$[c]	7200	11570	14100	36000	8000	17000	21000
$M_{n,SEC}$[d]	8100	12100	12700	29200	13300	26700	32700
Đ[d]	1.28	1.27	1.50	1.23	1.28	1.31	1.46

Evaporation induced mesoporous TiO_2 coating formation

To synthesize the mesoporous TiO_2 layers, the structure directing polymer was dissolved in THF. Micelle formation was induced by the dropwise addition of EtOH and finally the titania sol was formed in the same solution, by addition of the stabilizing acid HCl [20] and titanium tetra-isopropoxide. During spin coating, the solvents THF/EtOH evaporate and the Ti-sol starts to condense around the superstructure formed by the BCP. Crack formation was avoided by instant heat treatment of the coated thin layers at 75 °C, followed by a crystallization step at 450 °C for 3h. The mesoporous TiO_2 structure is supported up to a higher temperatures, compared to the case of Pluronic® surfactants, as evidenced from thermogravimetric analysis (TGA, Fig S10).

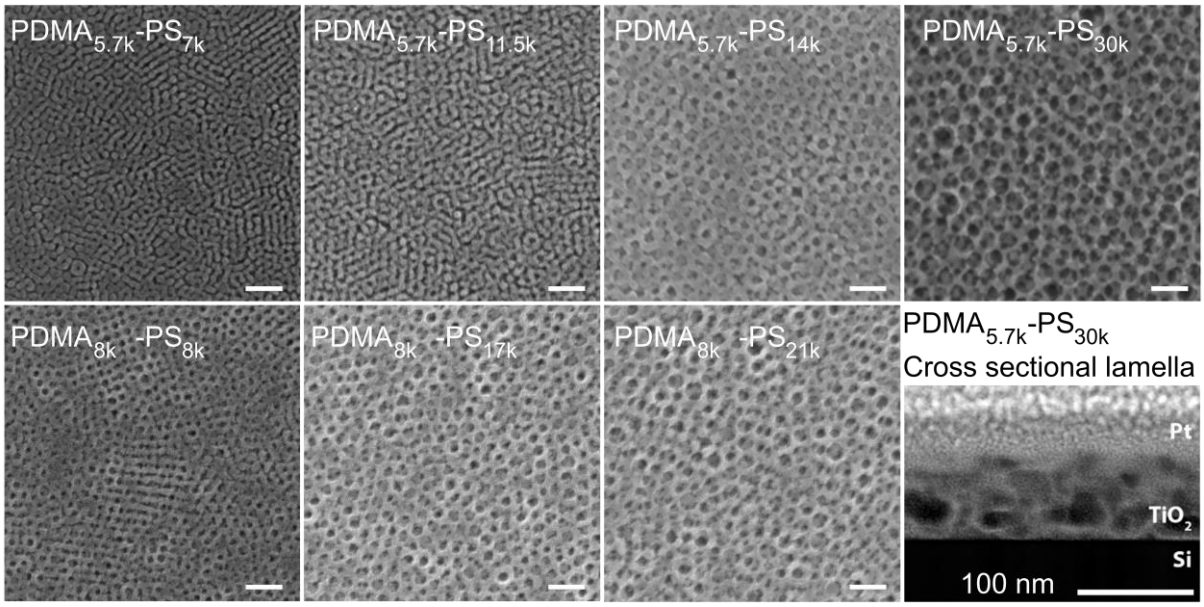

Figure 2: SEM images of meso-TiO_2 synthesized with the indicated PDMA-b-PS templates. The scale bar is set at 100 nm, and the average pore size and standard deviation was calculated from 150 measurements. In the bottom right corner image presents the cross-sectional analysis of a meso-TiO_2 thin layer synthesized with $PDMA_{5.7k}$-PS_{30k}.

Looking at the Scanning Electron Microscope (SEM) observations of the samples created with the different block copolymers in Figure 2, one can already expect the dependence of the pore size on the size of the non-polar PS polymer segment. To statistically prove this dependency, the influence of the molecular weight of the block segments on the pore size of the meso-TiO_2 was investigated with the statistical program "R" using a linear regression model. The strong and significant association between the polystyrene block size and the eventual pore size was

demonstrate by the linear regression obtained with an $R^2 = 0.9629$ and a p-value of $< 2.2*10^{-16}$, (Figure 3). The estimated regression function is given by the equation:

$$Y(\text{pore size nm}) = 1.532 * 10^{-3}\ \chi\ (\text{PS block size in Da}) \quad (1)$$

This equation indicates that by every addition of 10 styrene units to the polystyrene block, corresponding to an increase of 1040 g mol^{-1} in the molecular weight, an increase of 1.593 nm in pore size can be expected. As can be seen from this scatter plot, the mesopores made by $PDMA_{5.7k}$-b-PS_{14k} template seem to be significantly bigger than expected from the regression equation. This deviation in the pore size can be attributed to the high dispersity (Đ = 1.5) measured for this copolymer. The dispersity indicating the presence of a broader molecular weight distribution, a high value can explain this deviancy.

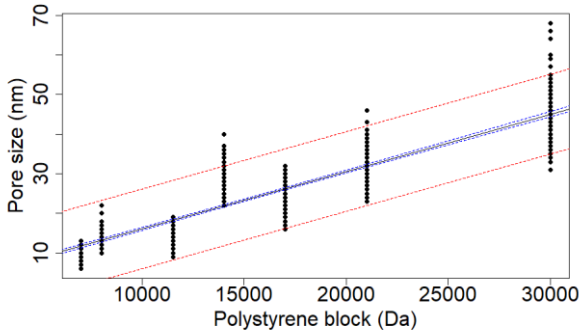

Figure 3: Scatter plot of the meso-TiO_2 pore sizes, as obtained for each PDMA-b-PS block copolymer template. The estimated regression function (black), the confidence interval for the mean(blue) and the 95 % prediction interval are indicated.

When the dispersity was included in the multiple regression analysis of the mesopores, still a good fit was obtained ($R^2 = 0.9645$, $p < 2.2 *10^{-16}$), with a regression equation of:

$$Y(\text{pore size in nm}) = 1.405* 10^{-3}\ \chi_1\ (\text{PS in Da}) + 1.84 * \chi_2\ (Đ) \quad (2)$$

This implicates the dispersity of a polymer will have an impact on the eventual pore size, although a minor one, as Đ doesn't vary greatly (here 1.2 – 1.5).

To investigate the influence of the dispersity and molecular weight of the block copolymer segments, aforementioned regression models were used on the standard deviation of the distribution of the pore diameters. As the standard deviation of the pores naturally increases with increasing pore sizes, one can observe the clear association between the polystyrene block size and the standard deviation of the pores (p-value = 0.000769 < 0.05, SI). However, of particular interest, the dispersity of the polymers doesn't show to significantly affect the pore standard deviation (p-value = 0.114).

It should be pointed out that performing regression analysis with dispersity of the SDA Đ, which is a measure of relative standard deviation, [50] to the standard deviation of the pores is an unfair comparison as the latter is not divided by its mean. By using equation 3 of dispersity, the relative standard deviation of the polymers can be calculated. Dividing the standard deviation of the pores by the mean pore size, the relative standard deviation of the mesopores can be calculated as well. By performing linear regression on the variables, no association is observed (p-value = 0.611) with the relative standard deviation of the polymers nor with any of the block copolymer segment sizes. This doesn't implicate that performing tight control over the dispersity of the block copolymer is not important, as it has been shown that the Đ will influence every aspect of the diblock copolymer self-assembly.[30] For example, more disperse block copolymers will have a stronger tendency to form *quasi*-vesicles,[29] which was however not observed here.

$$Đ = 1 + \frac{\sigma^2}{\mu^2} \quad (3)$$

The film thickness was obtained through cross-section analysis (Figure 2), where the meso-TiO_2 film had a thickness of only 75 nm. Through porosi-ellipsometry experiment of the latter thin film, the porosity was fitted to be 59 % (Figure S12). However, due to the experimental difficulties to obtain Brunauer–Emmett–Teller (BET) surface areas and pore size distributions for large pore (>50 nm) systems with porosi-ellipsometry, these were assessed using N_2-physisorption graphs of the meso-TiO_2 powders synthesized with the different $PDMA_{5.7k}$-PS_x copolymers (Fig S13). The BET surface areas of these powders ranged from up to 270 m^2g^{-1} for $PDMA_{5.1k}$-$PS_{11.5k}$ templated meso-TiO_2 to around 180 m^2g^{-1} for $PDMA_{5.7k}$-$PS_{30k,}$ indicating some pore collapse for the larger templates for meso-TiO_2 powders. Nevertheless these values are still high compared to other block copolymer-templated systems [19,1]. Looking at the powder X-ray diffraction (Fig 4) of a meso-TiO_2 powder, templated with $PDMA_{5.7k}$-PS_{30k}, one can see that the diffraction peaks are consisted with an anatase crystal phase (Figure 5).

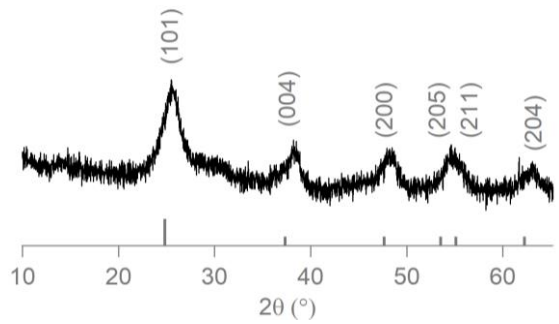

Figure 4: X-ray diffraction of a meso-TiO_2 powder templated with $PDMA_{5.7k}$-PS_{30k} matches the diffraction peak of the anatase crystal phase (PDF# 21-1272), indicated in gray

As such, we proved the viability of RAFT-synthetized PDMA-b-PS block copolymers as templates for the synthesis of meso-TiO_2, giving highly porous layers with pore-size control by controlling the polystyrene block size and the dispersity of the block copolymer. The pore relative standard deviation doesn't seem to be influenced by either the dispersity nor any of the block copolymer segment sizes. RAFT synthesized A-B structure directing agents do seem to be a viable alternative to ATRP/anionically polymerized SDA's for the synthesis of mesoporous TiO_2.

Photocatalytic properties

To evaluate the photocatalytic activity, a coated meso-TiO_2 layer prepared with the $PDMA_{5.7k}$-PS_{30k} template was applied to the continuous flow gas phase photocatalytic degradation of acetaldehyde in air. The activity is represented in terms of the steady-state decrease of the acetaldehyde levels and the steady state increase of CO_2 level, generated during UV illumination. To compare with a commercial TiO_2 product, 0.3 mg of aeroxide® P25 , corresponding to an equivalent amount of our meso-TiO_2 layer, was coated on a silicone wafer and exposed to the same conditions (Figure 5). Control experiments under dark conditions in

the presence of a catalyst film, as well as under UV illumination but in the absence of a catalyst film, showed no AcAl conversion.

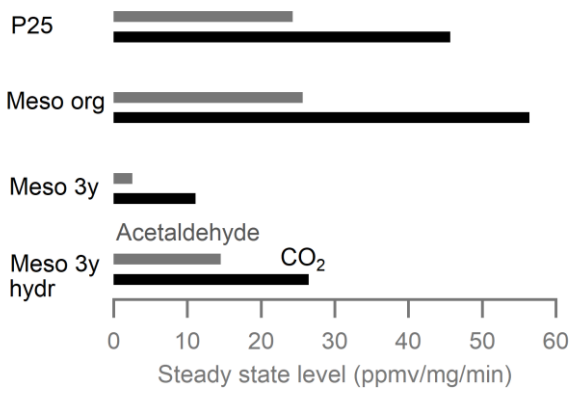

Figure 5: Photocatalytic degradation of acetaldehyde by meso-TiO_2 thin layer templated with $PDMA_{5.7k}$-PS_{30k} for the "Meso" samples: with respectively the original sample (Meso org), the sample after 3 years of storage in a dry atmosphere (Meso 3y) and the same sample after a quick wash with water (Meso 3y hydr). Finally the commercial powder aeroxide® P25 was also assessed. The grey levels are the steady-state decrease in the acetaldehyde level, the black levels the steady state CO_2 formation level.

From the photocatalytic steady state levels, one can see clearly that the activity of the original meso-TiO_2 $PDMA_{5.7k}$-PS_{30k} templated layer (Fig 6, Meso org) is marginally better compared to the P25 powder for the oxidation of acetaldehyde (steady state levels: 25.6 ppm mg^{-1} min^{-1} to 24.3 ppmv mg^{-1} min^{-1}). The steady state CO_2 formation level for "Meso org" is 56.1 ppmv mg^{-1} min^{-1}, which results in a slightly higher than expected 2:1 CO_2:acetaldehyde ratio, indicating probably another carbon source is being degraded on the surface of the thin layer as well, despite the photocatalytic pretreatment step built that is included in the testing protocol. This skewered ratio is even more apparent when the same layer was tested 3 years later (Fig 6, Meso 3y): the ratio of the steady state levels of CO_2:acetaldehyde relates to 4:1, clearly indicating another carbon source is being degraded. Also, the acetaldehyde reduction level was only 10% of the original value. This conundrum could be recently clarified by Diebold et. al. [51], who demonstrated the reduction in photocatalytic activity was due to the specific adsorption of air-bound carboxylic acids (formic acid/acetic acid) to the cationic adsorption sites, which rendered the surface hydrophobic and inaccessible to the contaminant. Indeed, when the "Meso 3y" layer was rinsed with bi-distilled H_2O (Fig 6, Meso 3y hydr), the photocatalytic activity immediately recovered to 57 % of its original level. In real-life applications, the constant treatment of rain and UV-light could prevent the specific adsorption of these air-bound carboxylic acids and the mesoporous layer would retain its original activity over a longer period [51]. Nevertheless, the

clear degradation of acetaldehyde shows the potential applicability of the thin layers of mesoporous TiO_2 by templating with PDMA-b-PS block copolymers, synthesized via RAFT.

Conclusion

A small library of PDMA-*b*-PS block copolymers with various PDMA/PS block ratios, molecular weight and dispersity indices were synthesized via reversible addition-fragmentation chain transfer polymerization. These block copolymers were successfully tested for the sol-gel synthesis of mesoporous TiO_2 thin layers, and pore size control was possible between 8 and 45 nm with the library synthesized here. Pore sizes were shown to be significantly correlated the polystyrene block size and the dispersity Đ of PDMA-b-PS. The pore size (relative) standard deviation was shown not to be affected by the dispersity of the block copolymer, which approved the use of RAFT-synthesized compared to ATRP/anionically synthesized surfactants. The meso-TiO_2 layers were crack-free and showed an anatase crystal phase. As a proof of concept the photocatalytic activity of the meso-TiO_2 thin layers was tested toward the degradation of acetaldehyde, a known model indoor pollutant. The thin film was aged over a period of 3 years and retained most of its activity. The original thin layer showed an activity slightly exceeding the commercially available Aeroxide® P25 photocatalyst.

Acknowledgements

Ghent University is acknowledged for funding the research presented in this paper. M. Meire and S. W. Verbruggen acknowledge the FWO-Flanders (Fund for Scientific Research-Flanders) for financial support. The authors thank Bernhard De Meyer for the SEC analysis, Hannes Rijckaert for the cross-section analysis, Tom Planckaert for BET analysis of the meso-TiO_2 powders, Jeroen Kint for the porosi-ellipsometry tests and Frank Driessen for the MALDI-TOF analysis.

References

1. Li W, Wu ZX, Wang JX, Elzatahry AA, Zhao DY (2014) A Perspective on Mesoporous TiO2 Materials. Chem Mat 26 (1):287-298. doi:10.1021/cm4014859
2. Yang PD, Zhao DY, Margolese DI, Chmelka BF, Stucky GD (1998) Generalized syntheses of large-pore mesoporous metal oxides with semicrystalline frameworks. Nature 396 (6707):152-155. doi:10.1038/24132
3. Taguchi A, Schuth F (2005) Ordered mesoporous materials in catalysis. Microporous Mesoporous Mat 77 (1):1-45. doi:10.1016/j.micromeso.2004.06.030

4. Smarsly B, Grosso D, Brezesinski T, Pinna N, Boissiere C, Antonietti M, Sanchez C (2004) Highly crystalline cubic mesoporous TiO2 with 10-nm pore diameter made with a new block copolymer template. Chem Mat 16 (15):2948-2952. doi:10.1021/cm0495966
5. Liu B, Louis M, Jin L, Li GH, He J (2018) Co-Template Directed Synthesis of Gold Nanoparticles in Mesoporous Titanium Dioxide. Chem-Eur J 24 (38):9651-9657. doi:10.1002/chem.201801223
6. Cao SB, Zhao YB, Qu T, Wang PP, Guan S, Xu YW, Rao F, Li YY, Chen AH, Iyoda T (2016) Ordered mesoporous crystalline titania with high thermal stability from comb-like liquid crystal block copolymers. RSC Adv 6 (61):55834-55841. doi:10.1039/c6ra10352a
7. Nakata K, Fujishima A (2012) TiO2 photocatalysis: Design and applications. J Photochem Photobiol C-Photochem Rev 13 (3):169-189. doi:10.1016/j.jphotochemrev.2012.06.001
8. Verbruggen SW (2015) TiO2 photocatalysis for the degradation of pollutants in gas phase: From morphological design to plasmonic enhancement. J Photochem Photobiol C-Photochem Rev 24:64-82. doi:10.1016/j.jphotochemrev.2015.07.001
9. Bach U, Lupo D, Comte P, Moser JE, Weissortel F, Salbeck J, Spreitzer H, Gratzel M (1998) Solid-state dye-sensitized mesoporous TiO2 solar cells with high photon-to-electron conversion efficiencies. Nature 395 (6702):583-585. doi:10.1038/26936
10. Hagfeldt A, Boschloo G, Sun LC, Kloo L, Pettersson H (2010) Dye-Sensitized Solar Cells. Chem Rev 110 (11):6595-6663. doi:10.1021/cr900356p
11. Yi CY, Li X, Luo JS, Zakeeruddin SM, Gratzel M (2016) Perovskite Photovoltaics with Outstanding Performance Produced by Chemical Conversion of Bilayer Mesostructured Lead Halide/TiO2 Films. Adv Mater 28 (15):2964-2970. doi:10.1002/adma.201506049
12. Stefano RM, Thomas W (2013) Titania supported hydrodesulphurisation catalysts.
13. Zhang Y, Yang QG, Yang XY, Deng YH (2018) One-step synthesis of in-situ N-doped ordered mesoporous titania for enhanced gas sensing performance. Microporous Mesoporous Mat 270:75-81. doi:10.1016/j.micromeso.2018.04.008
14. Fischer MG, Hua X, Wilts BD, Gunkel I, Bennett TM, Steiner U (2017) Mesoporous Titania Microspheres with Highly Tunable Pores as an Anode Material for Lithium Ion Batteries. ACS Appl Mater Interfaces 9 (27):22388-22397. doi:10.1021/acsami.7b03155
15. Li W, Wang F, Liu YP, Wang JX, Yang JP, Zhang LJ, Elzatahry AA, Al-Dahyan D, Xia YY, Zhao DY (2015) General Strategy to Synthesize Uniform Mesoporous TiO2/Graphene/Mesoporous TiO2 Sandwich-Like Nanosheets for Highly Reversible Lithium Storage. Nano Lett 15 (3):2186-2193. doi:10.1021/acs.nanolett.5b00291
16. Taffa DH, Kathiresan M, Walder L, Seelandt B, Wark M (2010) Pore size and surface charge control in mesoporous TiO2 using post-grafted SAMs. Phys Chem Chem Phys 12 (7):1473-1482. doi:10.1039/b921743f
17. Fuertes MC, Marchena M, Marchi MC, Wolosiuk A, Soler-Illia G (2009) Controlled Deposition of Silver Nanoparticles in Mesoporous Single- or Multilayer Thin Films: From Tuned Pore Fitting to Selective Spatial Location of Nanometric Objects. Small 5 (2):272-280. doi:10.1002/smll.200800894
18. Soler-Illia G, Azzaroni O (2011) Multifunctional hybrids by combining ordered mesoporous materials and macromolecular building blocks. Chem Soc Rev 40 (2):1107-1150. doi:10.1039/c0cs00208a
19. Fattakhova-Rohlfing D, Zaleska A, Bein T (2014) Three-Dimensional Titanium Dioxide Nanomaterials. Chem Rev 114 (19):9487-9558. doi:10.1021/cr500201c
20. Loreto S, Vanrompay H, Mertens M, Bals S, Meynen V (2018) The Influence of Acids on Tuning the Pore Size of Mesoporous TiO2 Templated by Non-Ionic Block Copolymers. Eur J Inorg Chem (1):62-65. doi:10.1002/ejic.201701266
21. Meynen V, Cool P, Vansant EF (2009) Verified syntheses of mesoporous materials. Microporous Mesoporous Mat 125 (3):170-223. doi:10.1016/j.micromeso.2009.03.046

22. Meire M, Verbruggen SW, Lenaerts S, Lommens P, Van Der Voort P, Van Driessche I (2016) Microwave-assisted synthesis of mesoporous titania with increased crystallinity, specific surface area, and photocatalytic activity. J Mater Sci 51 (21):9822-9829. doi:10.1007/s10853-016-0215-y
23. Lokupitiya HN, Jones A, Reid B, Guldin S, Stefik M (2016) Ordered Mesoporous to Macroporous Oxides with Tunable Isomorphic Architectures: Solution Criteria for Persistent Micelle Templates. Chem Mat 28 (6):1653-1667. doi:10.1021/acs.chemmater.5b04407
24. Stefik M, Song J, Sai H, Guldin S, Boldrighini P, Orilall MC, Steiner U, Gruner SM, Wiesner U (2015) Ordered mesoporous titania from highly amphiphilic block copolymers: tuned solution conditions enable highly ordered morphologies and ultra-large mesopores. J Mater Chem A 3 (21):11478-11492. doi:10.1039/c5ta02483h
25. Song L, Korstgens V, Magerl D, Su B, Froschl T, Husing N, Bernstorff S, Muller-Buschbaum P (2017) Low-Temperature Fabrication of Mesoporous Titania Thin Films. MRS Adv 2 (43):2315-2325. doi:10.1557/adv.2017.406
26. Wei J, Li YH, Wang MH, Yue Q, Sun ZK, Wang C, Zhao YJ, Deng YH, Zhao DY (2013) A systematic investigation of the formation of ordered mesoporous silicas using poly(ethylene oxide)-b-poly(methyl methacrylate) as the template. J Mater Chem A 1 (31):8819-8827. doi:10.1039/c3ta11469d
27. Nakatani H, Hamachi R, Fukui K, Motokucho S (2018) Synthesis and activity characteristics of visible light responsive polymer photocatalyst system with a styrene block copolymer containing TiO2 gel. J Colloid Interface Sci 532:210-217. doi:10.1016/j.jcis.2018.07.119
28. Xiao Y, You SS, Yao Y, Zheng T, Lin C, Roth SV, Muller-Buschbaum P, Steffen W, Sun LD, Yan CH, Gutmann JS, Yin MZ, Fu J, Cheng YJ (2013) Generalized Synthesis of Mesoporous Rare Earth Oxide Thin Films through Amphiphilic Ionic Block Copolymer Templating. Eur J Inorg Chem (8):1251-1257. doi:10.1002/ejic.201201524
29. Zhang Q, Lin JP, Wang LQ, Xu ZW (2017) Theoretical modeling and simulations of self-assembly of copolymers in solution. Prog Polym Sci 75:1-30. doi:10.1016/j.progpolymsci.2017.04.003
30. Lynd NA, Meuler AJ, Hillmyer MA (2008) Polydispersity and block copolymer self-assembly. Prog Polym Sci 33 (9):875-893. doi:10.1016/j.progpolymsci.2008.07.003
31. Thomas A, Schlaad H, Smarsly B, Antonietti M (2003) Replication of lyotropic block copolymer mesophases into porous silica by nanocasting: Learning about finer details of polymer self-assembly. Langmuir 19 (10):4455-4459. doi:10.1021/la0340807
32. Baskaran D, Muller AHE (2007) Anionic vinyl polymerization - 50 years after Michael Szwarc. Prog Polym Sci 32 (2):173-219. doi:10.1016/j.progpolymsci.2007.01.003
33. Feng HB, Lu XY, Wang WY, Kang NG, Mays JW (2017) Block Copolymers: Synthesis, Self-Assembly, and Applications. Polymers 9 (10):31. doi:10.3390/polym9100494
34. Sarkar A, Evans L, Stefik M (2018) Expanded Kinetic Control for Persistent Micelle Templates with Solvent Selection. Langmuir 34 (20):5738-5749. doi:10.1021/acs.langmuir.8b00417
35. Moad G, Rizzardo E, Thang SH (2009) Living Radical Polymerization by the RAFT Process - A Second Update. Aust J Chem 62 (11):1402-1472. doi:10.1071/ch09311
36. Chiefari J, Chong YK, Ercole F, Krstina J, Jeffery J, Le TPT, Mayadunne RTA, Meijs GF, Moad CL, Moad G, Rizzardo E, Thang SH (1998) Living free-radical polymerization by reversible addition-fragmentation chain transfer: The RAFT process. Macromolecules 31 (16):5559-5562. doi:10.1021/ma9804951
37. Keddie DJ (2014) A guide to the synthesis of block copolymers using reversible-addition fragmentation chain transfer (RAFT) polymerization. Chem Soc Rev 43 (2):496-505. doi:10.1039/c3cs60290g

38. Destarac M (2018) Industrial development of reversible-deactivation radical polymerization: is the induction period over? Polymer Chemistry 9 (40):4947-4967. doi:10.1039/C8PY00970H
39. Minehara H, Pitet LM, Kim S, Zha RH, Meijer EW, Hawker CJ (2016) Branched Block Copolymers for Tuning of Morphology and Feature Size in Thin Film Nanolithography. Macromolecules 49 (6):2318-2326. doi:10.1021/acs.macromol.5b02649
40. Sarkar A, Stefik M (2017) How to make persistent micelle templates in 24 hours and know it using X-ray scattering. J Mater Chem A 5 (23):11840-11853. doi:10.1039/c7ta01034f
41. Bianchi A, Mauri M, Bonetti S, Koynov K, Kappl M, Lieberwirth I, Butt HJ, Simonutti R (2014) Hierarchical self-assembly of PDMA-b-PS chains into granular nanoparticles: genesis and fate. Macromol Rapid Commun 35 (23):1994-1999. doi:10.1002/marc.201400414
42. Stefik M, Sai H, Sauer K, Gruner SM, DiSalvo FJ, Wiesner U (2009) Three-Component Porous−Carbon−Titania Nanocomposites through Self-Assembly of ABCBA Block Terpolymers with Titania Sols. Macromolecules 42 (17):6682-6687. doi:10.1021/ma900685e
43. Helms BA, Williams TE, Buonsanti R, Milliron DJ (2015) Colloidal Nanocrystal Frameworks. Adv Mater 27 (38):5820-5829. doi:10.1002/adma.201500127
44. Zhang JY, Deng YH, Gu D, Wang ST, She L, Che RC, Wang ZS, Tu B, Xie SH, Zhao DY (2011) Ligand-Assisted Assembly Approach to Synthesize Large-Pore Ordered Mesoporous Titania with Thermally Stable and Crystalline Framework. Adv Energy Mater 1 (2):241-248. doi:10.1002/aenm.201000004
45. Ferguson CJ, Hughes RJ, Nguyen D, Pham BTT, Gilbert RG, Serelis AK, Such CH, Hawkett BS (2005) Ab initio emulsion polymerization by RAFT-controlled self-assembly. Macromolecules 38 (6):2191-2204. doi:10.1021/ma048787r
46. Asapu R, Claes N, Bals S, Denys S, Detavernier C, Lenaerts S, Verbruggen SW (2017) Silver-polymer core-shell nanoparticles for ultrastable plasmon-enhanced photocatalysis. Appl Catal B-Environ 200:31-38. doi:10.1016/j.apcatb.2016.06.062
47. Deng SR, Verbruggen SW, He ZB, Cott DJ, Vereecken PM, Martens JA, Bals S, Lenaerts S, Detavernier C (2014) Atomic layer deposition-based synthesis of photoactive TiO2 nanoparticle chains by using carbon nanotubes as sacrificial templates. RSC Adv 4 (23):11648-11653. doi:10.1039/c3ra42928h
48. Verbruggen SW, Deng S, Kurttepeli M, Cott DJ, Vereecken PM, Bals S, Martens JA, Detavernier C, Lenaerts S (2014) Photocatalytic acetaldehyde oxidation in air using spacious TiO2 films prepared by atomic layer deposition on supported carbonaceous sacrificial templates. Appl Catal B-Environ 160:204-210. doi:10.1016/j.apcatb.2014.05.029
49. Rijckaert H, Pollefeyt G, Sieger M, Hanisch J, Bennewitz J, De Keukeleere K, De Roo J, Huhne R, Backer M, Paturi P, Huhtinen H, Hemgesberg M, Van Driessche I (2017) Optimizing Nanocomposites through Nanocrystal Surface Chemistry: Superconducting YBa2Cu3O7 Thin Films via Low-Fluorine Metal Organic Deposition and Preformed Metal Oxide Nanocrystals. Chem Mat 29 (14):6104-6113. doi:10.1021/acs.chemmater.7b02116
50. Harrisson S (2018) The downside of dispersity: why the standard deviation is a better measure of dispersion in precision polymerization. Polymer Chemistry 9 (12):1366-1370. doi:10.1039/C8PY00138C
51. Balajka J, Hines MA, DeBenedetti WJI, Komora M, Pavelec J, Schmid M, Diebold U (2018) High-affinity adsorption leads to molecularly ordered interfaces on TiO2 in air and solution. Science 361 (6404):786-789. doi:10.1126/science.aat6752